

Accelerating Chemo- and Regio-Selective Hydrogenation of Alkynes over Bimetallic Nanoparticles in a Metal-Organic Framework

Luyan Li, Weijie Yang, Qihao Yang, Qiaoqiao Guan, Junling Lu, Shu-Hong Yu, and Hai-Long Jiang

ACS Catal., **Just Accepted Manuscript** • DOI: 10.1021/acscatal.0c00177 • Publication Date (Web): 11 Jun 2020

Downloaded from pubs.acs.org on June 13, 2020

Just Accepted

“Just Accepted” manuscripts have been peer-reviewed and accepted for publication. They are posted online prior to technical editing, formatting for publication and author proofing. The American Chemical Society provides “Just Accepted” as a service to the research community to expedite the dissemination of scientific material as soon as possible after acceptance. “Just Accepted” manuscripts appear in full in PDF format accompanied by an HTML abstract. “Just Accepted” manuscripts have been fully peer reviewed, but should not be considered the official version of record. They are citable by the Digital Object Identifier (DOI®). “Just Accepted” is an optional service offered to authors. Therefore, the “Just Accepted” Web site may not include all articles that will be published in the journal. After a manuscript is technically edited and formatted, it will be removed from the “Just Accepted” Web site and published as an ASAP article. Note that technical editing may introduce minor changes to the manuscript text and/or graphics which could affect content, and all legal disclaimers and ethical guidelines that apply to the journal pertain. ACS cannot be held responsible for errors or consequences arising from the use of information contained in these “Just Accepted” manuscripts.

1
2
3
4
5
6
7 Accelerating Chemo- and Regio-Selective
8
9
10
11 Hydrogenation of Alkynes over Bimetallic
12
13
14
15 Nanoparticles in a Metal-Organic Framework
16
17
18
19

20 *Luyan Li,[†] Weijie Yang,[‡] Qihao Yang,[†] Qiaoqiao Guan,[†] Junling Lu,[†] Shu-Hong Yu,[†] and Hai-*
21 *Long Jiang^{*†}*
22
23

24
25
26 [†]Hefei National Laboratory for Physical Sciences at the Microscale, CAS Key Laboratory of Soft
27 Matter Chemistry, Collaborative Innovation Center of Suzhou Nano Science and Technology,
28 School of Chemistry and Materials Science, University of Science and Technology of China
29 Hefei, Anhui 230026, P. R. China
30
31
32
33

34
35 [‡]School of Energy and Power Engineering, North China Electric Power University, Baoding,
36 Hebei 071003, P.R. China
37
38

39
40 **KEYWORDS:** metal-organic framework, photothermal effect, alloy nanocrystals, plasmonic,
41 selective catalysis
42
43
44
45
46
47

48 **ABSTRACT:** Selective semi-hydrogenation of alkynes has been a long-term and significant
49 target yet remains a great challenge. Herein, bimetallic nanoparticles in a metal-organic
50 framework (MOF), *i.e.* CuPd@ZIF-8 composite, featuring a cubic CuPd core and a porous ZIF-8
51 shell, have been rationally fabricated for this end. Given the unique physicochemical properties,
52
53
54
55
56
57

1
2
3 the Cu nanocubes can not only convert solar energy into heat to accelerate the reaction but also
4
5 serve as the seed for *in situ* formation of Pd NPs on their external surface to regulate the
6
7 chemoselectivity of Pd active sites. The additional growth of MOF shell is helpful to stabilize
8
9 CuPd core and offer regioselectivity via steric hindrance effect. Ammonia borane provides active
10
11 hydrogen species to significantly boost the hydrogenation and ensure the high selectivity. As a
12
13 result, the CuPd@MOF exhibits high efficiency, featuring a turnover frequency (TOF, 6799 min⁻¹)
14
15 of 5 ~ 10⁵ times higher than that in previous reports, and high chemo- and regio-selectivity
16
17 toward the semi-hydrogenation of alkynes, in the presence of NH₃BH₃ as a hydrogen source,
18
19 under visible-light irradiation at ambient temperature.
20
21
22
23
24

25 INTRODUCTION

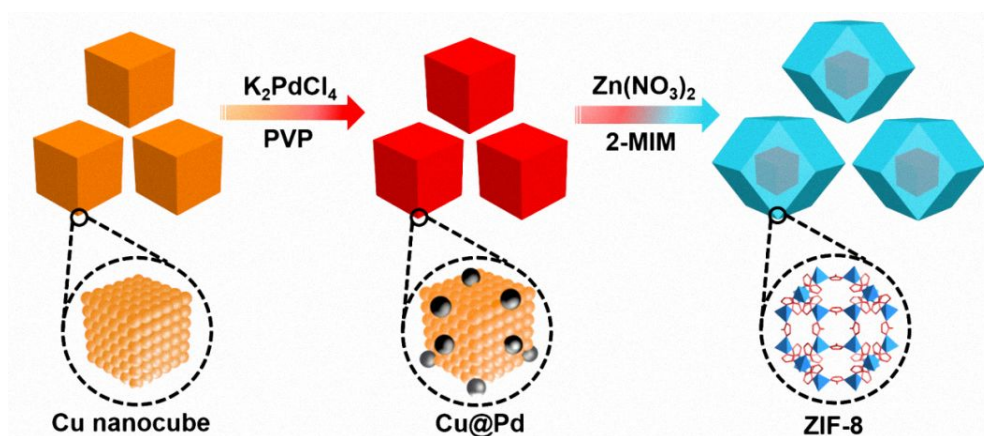
26
27
28 Selective semi-hydrogenation of alkynes to alkenes is of great importance and has attracted
29
30 particular attention in both academia and chemical industry, especially relevant to commodity
31
32 chemical production (e.g. purification of phenylethylene feeds for polymerization). Typically,
33
34 the alkynes, especially terminal alkynes, are prone to over-hydrogenation to alkanes because of
35
36 their high reactivity; the selective semi-hydrogenation of alkynes remains a particular
37
38 challenge.¹⁻¹⁰ To date, heterogeneous selective semi-hydrogenation reactions have been generally
39
40 investigated with metal-based catalysts in hydrogen (H₂) atmosphere. Amongst them, Pd-based
41
42 bimetallic catalysts are suggested to be most promising for this reaction. The classical Lindlar
43
44 catalyst, partially poisoning Pd with a secondary metal such as Pb to improve selectivity, remains
45
46 the choice in industry. However, the toxic lead, unsatisfied activity and high price are the driving
47
48 forces for the search of alternative catalysts. With the research effort, CuPd has been found based
49
50 on theoretical simulations to be very promising owing to its non-toxic and high selectivity for
51
52
53
54
55
56
57
58
59
60

1
2
3 hydrogenation reactions.^{11, 12} Unfortunately, experimental reports show that the semi-
4 hydrogenation reaction over CuPd usually requires high H₂ pressure and still causes over-
5 hydrogenation to alkanes at high conversion in the prolonged reaction time.^{1, 13-15} Therefore,
6
7
8 surpassing the limitation of the long-term “trade-off” effect to efficiently produce alkenes with
9
10 constant selectivity at high conversion level still poses a challenge by using the CuPd catalysts,
11
12
13 especially under ambient/moderate pressure, which is highly desired.
14
15
16

17
18 On the other hand, the increase of reaction temperature is a general way to accelerate the
19 kinetics of catalytic reactions. From the viewpoint of energy saving, the conversion of solar
20 radiation into heat energy, via the localized surface plasmon resonance (LSPR) of metal
21 catalysts,¹⁶⁻¹⁹ to elevate the reaction temperature is desirable. Although Cu nanoparticles (NPs)
22 possess LSPR-induced photothermal effect, it is rarely reported because they are easily oxidized
23 and/or chemically etched during the reaction/illumination.²⁰ To address this issue, encapsulating
24 Cu NPs into a porous material with appropriate pore sizes has shown to be an advisable
25 solution.²¹ The porous shell will not only prevent the Cu NPs from being further oxidized or
26 etched during the reaction, to some extent, but also facilitate the enrichment of substrates.
27 Moreover, uniform pore size might give rise to size-/regio-selective catalysis via the steric
28 hindrance effect. To meet these requirements, metal-organic frameworks (MOFs),²²⁻³⁰ a
29 relatively new class of crystalline porous materials with high surface area and tunable pore sizes,
30 might be ideal candidates.³¹⁻⁴⁸
31
32
33
34
35
36
37
38
39
40
41
42
43
44
45
46
47

48 Bearing the above considerations in mind, we have rationally fabricated a core-shell structured
49 MOF composite, namely CuPd@ZIF-8, which features cubic Cu supported Pd NPs together as a
50 core and a representative MOF, ZIF-8 (Zn(2-methylimidazole)₂),^{49, 50} as a shell (Scheme 1).
51 Particularly, to avoid high-pressure H₂ gas and tune the selective hydrogenation, ammonia
52
53
54
55
56
57

1
2
3 borane (NH_3BH_3), as a particular hydrogen source, has been introduced into the alkyne
4 hydrogenation system. Thanks to the plasmon-driven photothermal effect of Cu nanocubes
5 (NCs), the high Pd activity boosted by active hydrogen species from NH_3BH_3 , the
6 chemoselectivity influenced by Cu-Pd interaction while dominated by NH_3BH_3 hydrogen source,
7 and the protection and steric hindrance effect of ZIF-8 shell, the CuPd@ZIF-8 composite
8 exhibits excellent activity, both chemo- and regio-selectivity without “trade-off” effect, as well
9 as good recyclability, for alkyne semi-hydrogenation under visible light irradiation at ambient
10 temperature. Remarkably, the turnover frequency (TOF) of phenylacetylene semi-hydrogenation
11 reaches 6799 min^{-1} , surpassing all previously reported metal-based catalysts, and the high
12 selectivity can be well maintained with extended reaction time. Based on our knowledge of the
13 literature, this is an unusual report on a heterogeneous catalyst with high activity, chemo- and
14 regio-selectivity toward hydrogenation of alkynes.
15
16
17
18
19
20
21
22
23
24
25
26
27
28
29
30
31



Scheme 1. Schematic illustration showing the preparation process of CuPd@ZIF-8.

53 RESULTS AND DISCUSSION

54 The Cu NCs were prepared in H_2O in presence of $\text{CuCl}_2 \cdot 2\text{H}_2\text{O}$, glucose and hexadecylamine
55 (HAD).⁵¹ The Pd NPs were formed on the external surface of Cu NCs to give CuPd NCs via the
56
57
58
59
60

1
2
3 galvanic reaction between Pd²⁺ and Cu⁰ ($E_{\text{Pd}^{2+}/\text{Pd}} = +0.951$ eV vs SHE; $E_{\text{Cu}^{2+}/\text{Cu}} = +0.337$ eV vs
4 SHE). Following that, the Zn²⁺ and 2-methylimidazole were assembled onto the surface of CuPd
5 NCs with the help of interfacing polyvinyl pyrrolidone (PVP), leading to the formation of core-
6 shell structured CuPd@ZIF-8 composites (Scheme 1).
7
8
9
10
11

12
13 Powder X-ray diffraction (XRD) pattern of CuPd NCs shows two peaks at 43.5 and 50.7
14 degree, which can be assigned to the (111) and (200) diffractions of face-centered cubic Cu,
15 respectively, indicating the successful synthesis of Cu NCs (Figure S1a). The absence of
16 identifiable diffraction peak of Pd indicates the possibly low Pd content and/or small Pd sizes.
17
18 Powder XRD pattern of CuPd@ZIF-8 clearly demonstrates the formation of ZIF-8 with good
19 crystallinity (Figure S1a). N₂ sorption of CuPd@ZIF-8 indicates its high Brunauer-Emmett-
20 Teller (BET) surface area (1077 m²/g) and typical microporous character (Figure S1b). The
21 slight decrease in surface area compared to parent ZIF-8 (1296 m²/g) is ascribed to the mass
22 occupation of CuPd NCs.
23
24
25
26
27
28
29
30
31
32
33
34
35
36
37
38
39
40
41
42
43
44
45
46
47
48
49
50
51
52
53
54
55
56
57
58
59
60

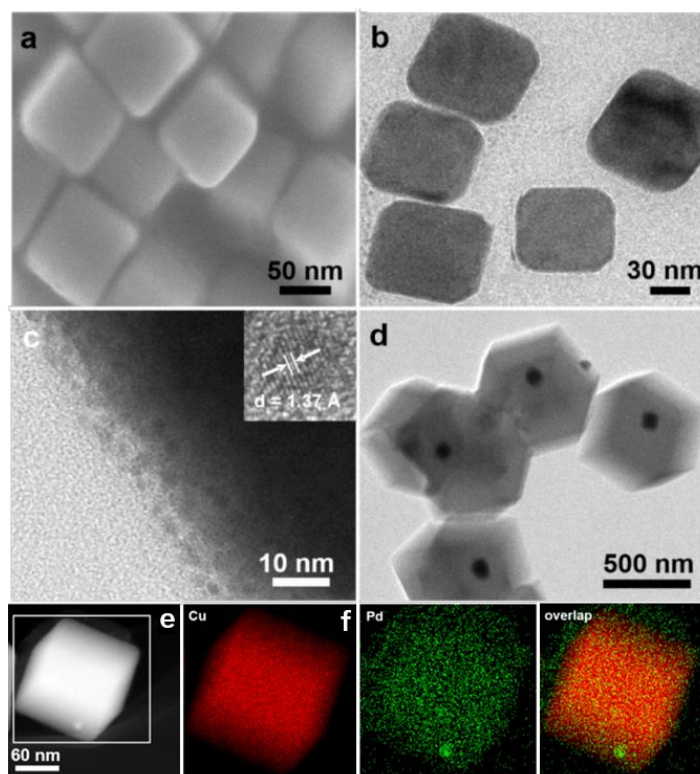
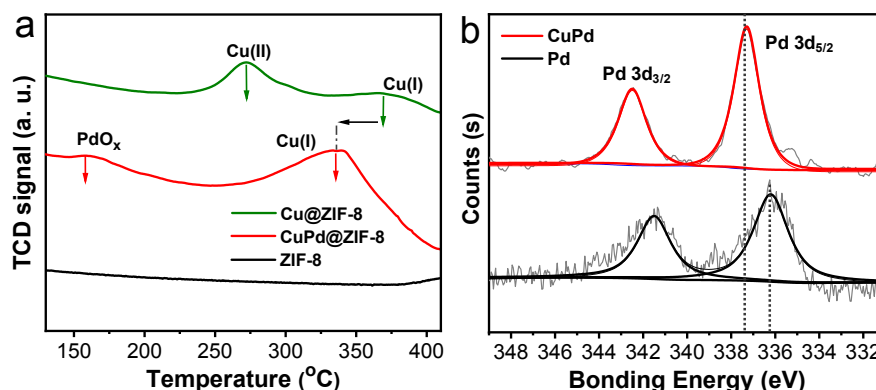


Figure 1. (a) SEM image of Cu NCs; TEM images of (b, c) CuPd NCs and (d) CuPd@ZIF-8. Inset of c: HRTEM image of Pd NPs; (e) HAADF-STEM of CuPd and (f) the corresponding elemental mapping of Cu (red), Pd (green).

Scanning electron microscope (SEM) observation shows that the Cu NCs have a regular shape with average sizes of 61 ± 6 nm (Figure 1a). Transmission electron microscopy (TEM), high-resolution TEM (HRTEM) and high-angle annular dark-field scanning TEM (HAADF-STEM) observation for CuPd NCs suggest that Pd NPs (~ 2.5 nm) are formed on the surface of Cu NCs and almost do not change the original morphology of the latter (Figure 1b-c, e, S2a). Elemental mapping results further support the uniform Pd dispersion on the Cu NCs (Figure 1f). The well observable lattice fringe with spacing of 1.37 \AA could be indexed to the (220) plane of Pd NPs (Figure 1c inset). The TEM image of CuPd@ZIF-8 indicates that the CuPd NCs are well

1
2
3 encapsulated by ZIF-8 shell and the size of an individual CuPd@ZIF-8 particle is 600-1000 nm
4
5 (Figure 1d, S2b). The actual contents of Cu and Pd are determined to be 5.5 mol% and 0.1
6
7 mol%, respectively, in CuPd@ZIF-8 composite by inductively coupled plasma atomic emission
8
9 spectroscopy (ICP-AES). The trace Pd loading signifies the low cost of this catalyst. Notably, the
10
11 LSPR-induced absorption of Cu NCs in 575-700 nm can be well inherited to CuPd@ZIF-8
12
13 composite (Figure S3), suggesting that the ZIF-8 shell can be successfully penetrated by light
14
15 irradiation. To investigate the interaction between Pd and Cu, the temperature-programmed
16
17 reduction (TPR) for CuPd@ZIF-8 was conducted. Two reduction peaks at around 160 °C and
18
19 340 °C can be assigned to the oxidative species of PdO and Cu₂O,¹⁴ respectively (Figure 2a).
20
21 Apparently, the reduction temperature of Cu₂O at ~340 °C for CuPd@ZIF-8 is lower than that
22
23 (369 °C) for Cu@ZIF-8, revealing the interaction between Pd and Cu. The reduction of Cu₂O in
24
25 CuPd@ZIF-8 might be promoted by the H₂ spillover from Pd to the neighboring Cu₂O.⁵² This
26
27 Cu-Pd interaction is further supported by X-ray photoelectron spectroscopy (XPS) data. The
28
29 3d_{5/2} peak for Pd⁰ shifts to the higher binding energy in CuPd due to the electron transfer from
30
31 Pd to Cu and the appearance of Cu²⁺ peak would be due to the partial oxidation of Cu in CuPd
32
33 NCs (Figure 2b, S4).¹⁹
34
35
36
37
38
39
40



41
42
43
44
45
46
47
48
49
50
51
52
53
54
55 **Figure 2.** (a) TPR profiles for Cu@ZIF-8, CuPd@ZIF-8 and ZIF-8; (b) XPS spectra of Pd 3d.
56
57
58
59
60

1
2
3 The above rationally fabricated CuPd@ZIF-8 composite is expected to afford excellent
4 performance toward selective hydrogenation of alkynes under light irradiation at ambient
5 temperature. The phenylacetylene (**1a**) hydrogenation was firstly investigated to optimize the
6 reaction parameters (Figure 3). As expected, a high selectivity (97%) to phenylethylene (**1b**) can
7 be achieved over CuPd@ZIF-8 in H₂ atmosphere at room temperature, which is distinctly
8 different from the poor selectivity (<1%) over Pd@ZIF-8 (Figure 3, Figure S5). The results
9 suggest that the introduction of Cu is crucial to the high selectivity, probably due to the lower
10 adsorption stability between alkene and the formed Pd NPs outside Cu NCs.¹ Unfortunately, the
11 conversion of **1a** over CuPd@ZIF-8 is only 19% under these conditions, which is even lower
12 than Pd@ZIF-8, as the Cu introduction reduces the adsorption energy of substrates and
13 suppresses the H₂ dissociation based on the previous reports.^{1, 53} The photothermal effect of Cu
14 nanocubes in the catalyst is thought to be able to improve the conversion. To evaluate the
15 efficiency of photothermal conversion of CuPd@ZIF-8, the temperature change in the solution
16 along with time is detected. Results clearly show that light energy can be efficiently converted
17 into heat in the presence of CuPd@ZIF-8 (Figure S6). As expected, by simply introducing light
18 irradiation, the conversion of **1a** over CuPd@ZIF-8 can be promoted to 40%, reflecting the great
19 contribution of photothermal effect (Figure 3). While the activity is improved, the selectivity
20 slightly decreases to 90% at this conversion (40%), and continues to fall off along with higher
21 conversion (Figure S7), in H₂ atmosphere. The results indicate that, though the contribution of
22 Cu-Pd interaction in CuPd@ZIF-8, the over-hydrogenation trend might be hardly avoidable in
23 H₂ atmosphere, similar to the results in previous reports.^{1, 15}
24
25
26
27
28
29
30
31
32
33
34
35
36
37
38
39
40
41
42
43
44
45
46
47
48
49
50
51
52
53
54
55
56
57
58
59
60

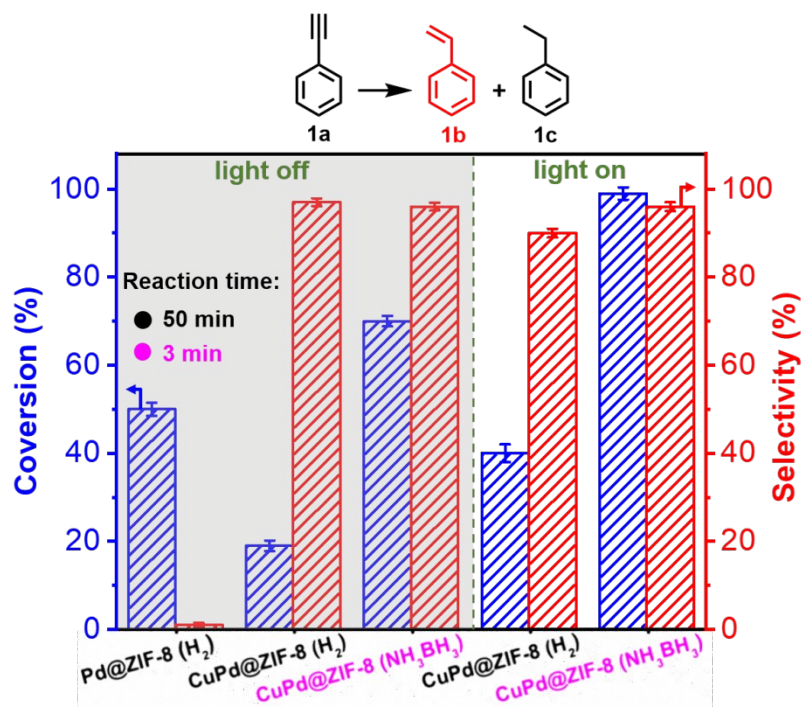


Figure 3. (a) Semi-hydrogenation of phenylacetylene in CH₃OH with hydrogen donor of H₂ balloon (or NH₃BH₃) over Pd@ZIF-8 (or CuPd@ZIF-8) in the absence (left side, with grey background) or presence (right side, no background) of light irradiation (>400 nm, 160 mW/cm²).

The above results drive us to explore suitable hydrogen source to afford constantly excellent selectivity at even high conversions toward the semi-hydrogenation of alkynes. Ammonia borane (NH₃BH₃) with high hydrogen content of 19.6 wt% has been recognized as a highly potential hydrogen storage medium.⁵⁴⁻⁵⁹ The NH₃BH₃ displays excellent solubility in methanol to *in situ* generate active hydrogen species, facilitating subsequent hydrogenation.⁵⁷⁻⁵⁹ Therefore, it is assumed that NH₃BH₃ might be a suitable hydrogen source to meet this challenge. The alcoholysis of NH₃BH₃ over CuPd@ZIF-8 was found to steadily proceed, producing pure H₂, and the reaction can be promoted under the light irradiation (Figure S8). Encouraged by this, the semi-hydrogenation of **1a** was examined with NH₃BH₃ instead of H₂. Significantly, in reference

to the 70% conversion of **1a**, light irradiation further leads to its almost complete conversion (99%) with 96% selectivity to **1b** within 3 min, based on the CuPd@ZIF-8 catalyst (Figure 3). This much higher activity than that using H₂ gas discussed above implies that NH₃BH₃ might generate special active hydrogen species to boost the reaction. In contrast, Pd@ZIF-8 gives only 68% selectivity and no reaction occurs with ZIF-8, implying the importance of Pd for the activity while Cu for promoting the selectivity (Table S1). To our delight, the ZIF-8 shell almost does not bring effects on the catalytic rate, based on the comparison of phenylacetylene hydrogenation kinetics over CuPd NCs and CuPd@ZIF-8 (Figure S9). The transport limitation of ZIF-8 has been further excluded by examining the yield dependence on the catalyst amount (Figure S10). The TOF of CuPd@ZIF-8 is calculated to be 6799 min⁻¹, which represents the highest value among ever reported metal catalysts for this reaction (Table S2). The high efficiency implies that the introduction of NH₃BH₃ might boost the conversion by the sufficient contact between the substrate and the hydrogen donor, which *in situ* generates hydrogen active species.⁵⁷

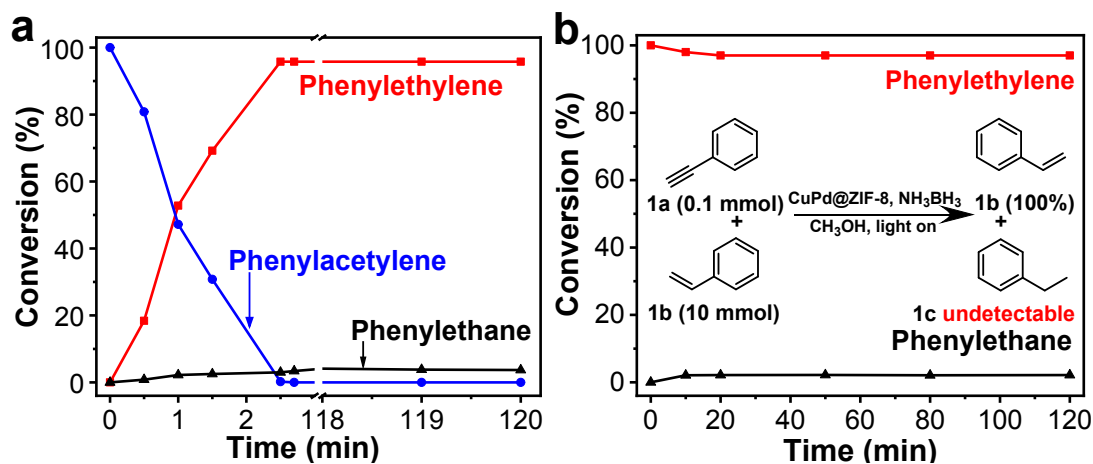


Figure 4. Time-dependent conversion of the hydrogenation of (a) phenylacetylene or (b) phenylethylene using CuPd@ZIF-8 with NH₃BH₃ as the hydrogen source under light irradiation

1
2
3 at ambient temperature. Inset of b: selective reduction of a 1:100 mixture of phenylacetylene and
4 phenylethylene.
5
6

7
8 More importantly, the selectivity shows an apparent decrease in the prolonged reaction time in
9 H₂ atmosphere, while almost no over-hydrogenated product can be detected even the reaction
10 time length is extended to 2 h in presence of NH₃BH₃ (Figure 4a, S11). This point has been
11 further clarified by employing **1b** as the reactant for hydrogenation over CuPd@ZIF-8, where
12 almost no phenylethane (**1c**) can be produced (Figure 4b). The results unambiguously
13 demonstrate that, in addition to the Cu in the catalyst, NH₃BH₃ also plays a critical role in the
14 high chemoselectivity for the semi-hydrogenation of alkyne. Encouraged by these results, the
15 experiment, the removal of a small amount of **1a** (0.1 mmol) from **1b** (10 mmol), which
16 represents the important purification process in steam cracking of alkenes (usually containing a
17 small fraction of alkyne impurities) in industry,^{60, 61} was investigated. Strikingly, **1a** can be
18 completely converted to **1b** rapidly without over-hydrogenation to **1c** (Figure 4b inset). These
19 results are very exciting and can be achieved in very few reports,^{60, 61} as the conventional
20 catalysts (such as the commercial Lindlar catalyst) and/or hydrogen gas usually result in rapid
21 over-hydrogenation to alkanes with prolonged reaction time.
22
23
24
25
26
27
28
29
30
31
32
33
34
35
36
37
38
39
40

41 To get insight into the hydrogenation process over the CuPd@ZIF-8 in the presence of
42 NH₃BH₃, controlled experiments and density functional theory (DFT) calculations were carried
43 out. The dependency of the reaction rate on the NH₃BH₃ amount toward the hydrogenation of **1a**
44 suggests that it follows the first-order reaction, manifesting that NH₃BH₃ is truly participated in
45 the reaction (Figure 5a).⁶² To understand the adsorption behavior of phenylacetylene (C₈H₆) and
46 NH₃BH₃ substrates over the active sites, their adsorption on the catalyst surface has been
47 investigated through calculating the adsorption energy and adsorption configuration (Figure 5b,
48
49
50
51
52
53
54
55
56
57
58
59
60

S12). The adsorption energy of C_8H_6 on Pd site is -2.43 eV, apparently larger than that of NH_3BH_3 (-1.49 eV), which suggests the stronger interaction between C_8H_6 and Pd sites. Accordingly, C_8H_6 is preferentially adsorbed on Pd sites. In reverse, NH_3BH_3 is mainly adsorbed on Cu sites, due to its larger adsorption energy (-1.38 eV) than that of C_8H_6 (-0.61 eV) on Cu sites.

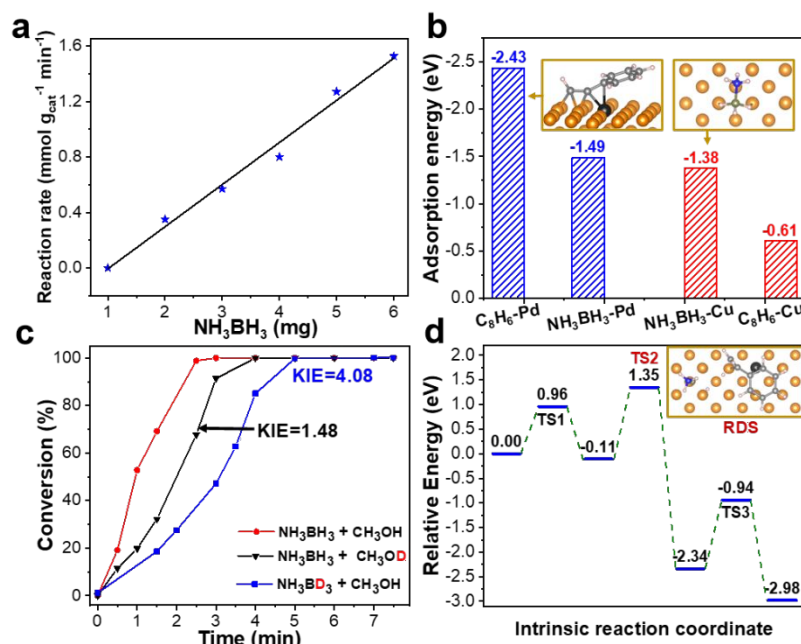


Figure 5. (a) Dependency of the reaction rate on the amount of NH_3BH_3 . The correlation coefficient (R^2) is 0.98. (b) Adsorption energy of C_8H_6 and NH_3BH_3 on Pd and Cu sites, respectively. (c) Semi-hydrogenation of phenylacetylene using $CuPd@ZIF-8$ with NH_3BH_3 in CH_3OH (red), NH_3BH_3 in CH_3OD (black) and NH_3BD_3 in CH_3OH (blue). (d) Energies of intermediates and TSs in the mechanism of phenylacetylene hydrogenation to afford the 1st molecule of alkene (step I) over $CuPd@ZIF-8$ in presence of NH_3BH_3 based on DFT calculations. Pd atom (black), Cu atom (orange).

1
2
3 Subsequently, the deuterium-labeling experiments were conducted to figure out the real role of
4 NH_3BH_3 in the reaction (Figure S13, S14). Whatever NH_3BD_3 or ND_3BH_3 is introduced into
5 CH_3OH , the deuterated phenylethylene can be obtained (Figure S14), clearly approving the
6 cleavage of both B-H and N-H bonds is involved in the reaction and probably the generated
7 hydrogen species ($\text{H}^{\delta-}$ and/or $\text{H}^{\delta+}$)⁵⁴ participate in the formation of phenylethylene product.
8 Furthermore, the ratio (4.08) of rate constants, KIE (K_L/K_H), which falls in the value range (2-7)
9 of the primary kinetic isotope effect,⁶³ for the reactions involving light (K_L) and heavy (K_H)
10 isotopically substituted ammonia borane (NH_3BD_3), demonstrating that the activation of B-H
11 bond is the rate-determining step (RDS) in the reaction and revealing that the generated $\text{H}^{\delta-}$
12 might be involved in the reaction (Figure 5c). In contrast, the KIE of 1.48 for the reactions
13 involving isotopically substituted methanol (CH_3OD) suggests that the O-H activation in
14 methanol would not be the RDS in the reaction.
15
16
17
18
19
20
21
22
23
24
25
26
27
28
29
30

31 In sharp contrast to the deuterated NH_3BH_3 experiments above, no H-D exchange takes place
32 and all the H atoms in phenylethylene can be detected in the ^1H NMR spectrum with NH_3BH_3 in
33 CD_3OD solvent (Figure S15), excluding the possibility of H atom in alkene product originated
34 from CH_3OH . This is completely different from the reported *in situ* H_2 generation from NH_3BH_3
35 for subsequent hydrogenation process in previous examples,^{60, 61} in which the H_2 is originated
36 from both B-H cleavage and the other proton in CH_3OH .⁵⁴ According to the reported work,⁶⁴ it is
37 assumed that the active hydrogen species from B-H and N-H cleavage are able to react with the
38 alkyne group directly to give product, which is supported by the fact that negligible hydrogen gas
39 production can be detected during our reaction (Figure S16).
40
41
42
43
44
45
46
47
48
49
50
51
52

53 To further get clear how the hydrogenation process takes place, we propose a plausible
54 mechanism by resorting DFT calculation and above experimental results (Figure S17, S18). It is
55
56
57
58
59
60

1
2
3 proposed that the ideal alkyne hydrogenation in the presence of NH_3BH_3 involves three steps (I,
4 II, III) and generates three molar alkenes by consuming one molar NH_3BH_3 . The process (step I)
5 of generating the 1st molecule of alkene has been confirmed by the DFT calculations. First of all,
6 NH_3BH_3 and C_8H_6 are adsorbed onto the Cu and Pd surfaces, respectively. Then, the breaking of
7 B-H bond in NH_3BH_3 gives the first hydrogen species ($\text{H}^{\delta-}$) on the Cu surface, which
8 nucleophilically attacks the $\text{C}\equiv\text{C}$ bond (**TS1**) (Figure S17c). Meanwhile, the other H atom ($\text{H}^{\delta-}$)
9 is also released by the second B-H breaking, co-participating in the formation of the 1st molecule
10 of alkene, which is identified as the RDS process with an energy barrier of 1.46 eV (**TS2**)
11 (Figure 5d, S17e). The new ammonia alkoxyborane complex ($\text{BH}_2=\text{NH}_2$) is subsequently created
12 by transferring one H atom from $-\text{NH}_3$ to $-\text{BH}$ (**TS3**), which is validated by the infrared
13 spectroscopy (Figure S17g, S19). The 2nd molecule of alkene is produced following the similar
14 process as the first step (I) by consuming two $\text{H}^{\delta-}$ species from two B-H bond cleavage (Figure
15 S17i-j, S18). The 3rd molecule of alkene is generated via obtaining one H atom from the B-H
16 breaking. It is supposed that the other proton is from the N-H breaking via an inner-sphere
17 addition mechanism (Figure S18).⁶⁴ This assumption is supported by the deuterated experiments
18 (ND_3BH_3 and CD_3OD), which indicate the hydrogen species from N-H cleavage, but not proton
19 from CH_3OH , participates in the production of alkene (Figure S14, S15). After producing the
20 three molecules of alkene, $\text{NH}_4\text{B}(\text{OCH}_3)_4$ is accordingly generated, as evidenced by the ^{11}B
21 NMR spectrum for the mixture (Figure S20).
22
23
24
25
26
27
28
29
30
31
32
33
34
35
36
37
38
39
40
41
42
43
44
45
46

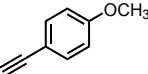
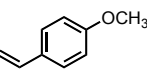
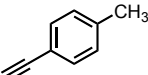
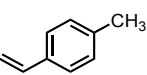
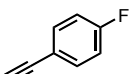
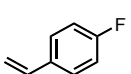
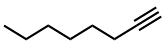
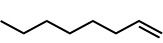
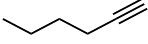
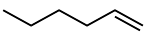
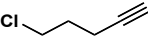
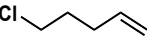
47 From the above experimental and calculated results, it is clear that the active hydrogen species
48 ($\text{H}^{\delta-}$ and $\text{H}^{\delta+}$) from B-H and N-H cleavage directly react with alkynes instead of producing H_2 .
49 Given the weak interaction between the polar hydrogen species and alkenes,⁶² the hydrogenation
50 of alkenes is unfavorable, suppressing their over-hydrogenation and thus resulting in high
51
52
53
54
55
56
57
58
59
60

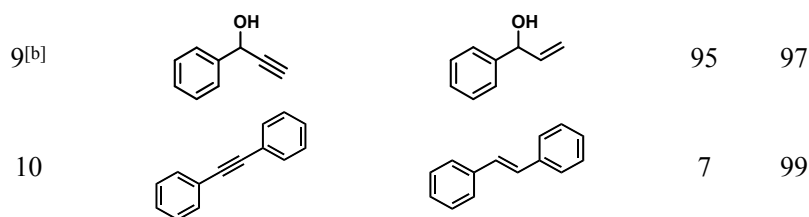
selectivity to alkenes. Therefore, such hydrogenation process over CuPd@ZIF-8 is based on the reaction between **1a** and polar hydrogen species ($H^{\delta-}$ and $H^{\delta+}$) from NH_3BH_3 , distinctly different from the reaction in H_2 atmosphere.

To further investigate the stability and reusability of the catalyst, recycling experiments have been also carried out. To our delight, the activity of CuPd@ZIF-8 is well maintained in the five consecutive runs, indicating its great recyclability and stability (Figure S21a, b). In comparison, the conversion over CuPd NCs, in the absence of ZIF-8 shell protection, sharply decreases during the three cycles due to the surface oxidation and possible chemical etching of Cu NCs (Figure S21c, d).^{20, 31}

Table 1. Selective hydrogenation of different alkynes over CuPd@ZIF-8.^[a]

$$R_1-C\equiv C-R_2 \longrightarrow R_1-CH=CH-R_2$$

Entry	Substrate	Product	Con. (%)	Sel. (%) ^[c]
1			97	96
2			98	97
3			98	94
4			97	96
5			93	97
6			92	94
7			93	95
8			94	95



^a Reaction conditions: substrate (0.1 mmol), time (5 min), CuPd@ZIF-8 (1 mg, Pd: 0.1 mol%), CH₃OH (6 mL), NH₃BH₃ (5 mg), light: >400 nm, 160 mW/cm². ^b Time (10 min). [^c] Catalytic reaction products were analyzed and identified by gas chromatography.

Encouraged by the outstanding catalytic performance of CuPd@ZIF-8 towards the semi-hydrogenation of phenylacetylene, a variety of alkynes with different functional groups have been investigated (Table 1). Delightedly, various terminal aryl alkynes with electron-donating (-OCH₃ and -CH₃) or electron-withdrawing (-F) substituents can be completely transformed to the corresponding alkenes with high chemoselectivity (>94%) (entries 1-5). Moreover, the selective hydrogenation of aliphatic alkynes can be also achieved with excellent selectivity (>94%), indicating the great substrate tolerance of the catalyst (entries 6-9). On the contrary, the hydrogenation of diphenylacetylene was greatly restrained and only 7% conversion was achieved over CuPd@ZIF-8 (entry 10). The result indicates that the transformation of internal alkynes to the corresponding alkenes is impeded possibly due to the steric hindrance by the small pore size of ZIF-8, which makes the internal carbon-carbon triple bond hardly accessible to the Pd active sites. Inspired by this, the hydrogenation of the substrate with multiple functional groups, phenylpropionaldehyde, is attempted to get the alkynol, 2-propyn-1-ol, which is an important corrosion inhibitor in petrochemical industry (Table 2).⁶⁵ Incredibly, the desired product is obtained with 98% selectivity over CuPd@ZIF-8 (entry 1). In contrast, both carbon-carbon triple bond and terminal aldehyde group are reduced over the CuPd catalyst (entry 2). This suggests that the small pore size of ZIF-8 allows the terminal aldehyde group only but restrains the internal triple bond to interact with the Pd sites. Therefore, ZIF-8 shell not only contributes to

the stabilization of CuPd NCs but also offers the high regioselectivity via the space steric hindrance.

Table 2. Selective hydrogenation of phenylpropiolaldehyde over CuPd@ZIF-8 and CuPd^a.

Entry	Catalyst	Conv. (%)	Yield (%) ^b		
			c	d	e
1	CuPd@ZIF-8	>99	98	2	-
2	CuPd	>99	68	32	-

^aReaction conditions: substrate (0.1 mmol), time (12 min), CuPd@ZIF-8 (Pd: 0.1 mol%); CuPd (Pd: 0.1 mol%), CH₃OH (4.5 mL), H₂O (1.5 mL), NH₃BH₃ (7.8 mg), light: >400 nm, 160 mW/cm². ^bCatalytic reaction products were analyzed and identified by gas chromatography.

CONCLUSION

In summary, we have rationally fabricated a core-shell CuPd@ZIF-8 composite, featuring a cubic CuPd core and a MOF shell, for selective hydrogenation of alkynes. In the catalyst, the Cu not only achieves plasmonic photothermal conversion but also regulates the Pd electronic state to improve the catalytic chemoselectivity; the MOF stabilizes the CuPd NCs and enables regioselective hydrogenation of alkynes via steric hindrance effect. Thanks to the well dispersed Pd site, the Cu photothermal effect, and the *in situ* generated active hydrogen species from NH₃BH₃ that is well soluble in CH₃OH solvent, the hydrogenation of alkynes can be greatly boosted. Particularly, instead of traditional H₂ gas, the active hydrogen species generated from the alcoholysis of NH₃BH₃ ensure the high chemoselectivity in the hydrogenation of alkynes or alkene/alkyne mixture even over extended reaction time. As a result, the CuPd@ZIF-8 is capable of catalyzing the hydrogenation of alkynes to alkenes with high chemo- and regio-selectivity, good recyclability and extremely high activity, featuring the highest TOF value reported thus far,

1
2
3 toward phenylacetylene semi-hydrogenation. This work opens a new avenue to the rational
4 design of highly efficient, chemo- and regio-selective composite catalysts and suitable catalytic
5 systems toward high-performance catalysis.
6
7
8
9

10 **EXPERIMENTAL SECTION**

11
12
13 **Preparation of Cu nanocubes:** The Cu NCs were prepared according to the previous work
14 with minor modifications.⁵¹ Typically, 52.5 mg of CuCl₂·2H₂O, 50 mg of glucose, 225 mg of
15 HAD and 25 mL water were mixed in a 50 mL round-bottom flask and capped. The mixture
16 solution was magnetically stirred at room temperature for 12 h. Then the flask was transferred
17 into an oil bath and heated at 100 °C for at least 6 h under magnetic stirring. As the reaction
18 proceeded, the color of the solution was changing from blue to red-brown. After reaction, the
19 product was harvested by centrifugation and washed six times with hot water (65 °C). Finally,
20 the sample was dispersed into 5 mL hot water (2 mg/mL).
21
22
23
24
25
26
27
28
29
30

31
32 **Preparation of CuPd nanocubes:** The obtained Cu nanocubes solution (1 mL) was diluted
33 into 10 mL deionized water in a 25 mL round-bottom flask, followed by the addition of 50 mg
34 PVP under vigorous stirring for 12 h. Then, 1 mL (0.91 M) of K₂PdCl₄ aqueous solution was
35 injected into the Cu nanocubes solution using a syringe pump at a rate of 0.25 mL/min under
36 stirring for 12 h. After the galvanic reaction, the obtained product was collected via
37 centrifugation and dispersed into 1 mL methanol (2 mg/mL).
38
39
40
41
42
43
44
45

46 **Preparation of CuPd@ZIF-8:** Typically, CuPd nanocubes solution (1 mL) and the methanol
47 solution of zinc nitrate (25 mM, 15 mL), were mixed at room temperature under N₂ bubbling for
48 5 min, then the equivalent volume of methanol solution of 2-methylimidazole (25 mM, 15 mL)
49 was added to react at 40 °C for 30 min in a water bath with a N₂ balloon without stirring.⁶⁶ The
50 resultant composite was collected by centrifugation and washed twice with methanol. The
51
52
53
54
55
56
57
58
59
60

1
2
3 synthesized red-brown powder was further dried overnight at 333 K under dynamic vacuum and
4
5 dispersed into 4 mL methanol (1 mg/mL).
6

7
8 **Preparation of Pd@ZIF-8:** The Pd nanoparticles (~3 nm) were prepared firstly according to
9
10 the reported work with minor modification.⁶⁷ Typically, 105 mg of Polyvinylpyrrolidone (PVP,
11
12 ~55000 Mw), 60 mg of ascorbic acid and 5 mg of KBr were dispersed into 8 mL of deionized
13
14 water and preheated at 80 °C for 10 min. Then, 3 mL of K₂PdCl₄ (57 mg) aqueous solution was
15
16 added and reacted for 3 hours at 80 °C. The Pd nanoparticles were collected via centrifugation
17
18 and washed with acetone for five times. Finally, the obtained Pd nanoparticles are dispersed into
19
20 6 mL of deionized water (1 mg/mL). To synthesize Pd@ZIF-8, 750 µL of Pd nanoparticles
21
22 solution (1 mg/mL) was mixed with the methanol solution of zinc nitrate (Zn(NO₃)₂·6H₂O, 1.069
23
24 g, 15 mL), then the equivalent volume of methanol solution of 2-methylimidazole was added
25
26 (C₄H₆N₂, 1.61 g, 15 mL). The obtained mixed solvent reacted for 10 hours at room temperature.
27
28 After the reaction, the gray powder was collected via centrifugation and washed three times with
29
30 methanol. Finally, the obtained product was dried in vacuum oven at 60°C for 12 h.
31
32
33
34

35
36 **Preparation of ND₃BH₃ and NH₃BD₃:** ND₃BH₃ was prepared according to the reported
37
38 method with minor modifications.⁶⁸ Firstly, 30 mg NH₃BH₃ and 2 mL CD₃OD were added in a 5
39
40 mL round bottom flask and vigorously stirred for 4 h at room temperature, then ND₃BH₃ was
41
42 obtained after removing the solvent in vacuum. NH₃BD₃ was also prepared according to the
43
44 reported method. Briefly, NaBD₄ (100 mg) and (NH₄)₂SO₄ (315.7 mg) were added to a 100 mL
45
46 three-neck round bottom flask. Then, 14 mL THF was added and the mixture was vigorously
47
48 stirred at 40 °C for 2 h. Subsequently, it was cooled down to room temperature, filtered and dried
49
50 under vacuum to give NH₃BD₃ powder.
51
52
53
54
55
56
57
58
59
60

1
2
3 **Photothermal effect evaluation:** In general, a mixture of 1 mg catalyst (1 mL, 1 mg/mL) and
4 6 mL methanol was placed in a two-necked round-bottomed flask (25 mL) and capped. The
5 mixture was irradiated under 160 mW/cm² light with a 300 W Xe lamp and magnetic stirring.
6
7 Then, the temperature of solution was detected and recorded every 10 min to give the time-
8 temperature curve.
9

10
11 **Catalytic performance evaluation for the dehydrogenation of ammonia borane**
12 **(NH₃BH₃):** In general, a mixture of 1 mg catalyst (1 mL, 1 mg/mL) and 5 mL methanol was
13 placed in a two-necked round-bottomed flask (25 mL) and capped. The mixture was irradiated
14 under 160 mW/cm² light with a 300 W Xe lamp. A gas burette filled with water was connected
15 to the reaction flask to measure the volume of hydrogen evolved. The reaction started when
16 NH₃BH₃ (5 mg) was added into the flask. The volume of the evolved hydrogen gas was
17 monitored by recording the displacement of water in the gas burette. This reaction was
18 completed when there was no more gas generated.
19
20
21
22
23
24
25
26
27
28
29
30
31

32
33 **Catalytic performance evaluation of ZIF-8 and Pd@ZIF-8 for hydrogenation of**
34 **phenylacetylene in the presence of NH₃BH₃:** Typically, a mixture of Pd@ZIF-8 or ZIF-8 (1
35 mg), 0.1 mmol phenylacetylene, 5 mL methanol was placed in a two-necked round-bottomed
36 flask (25 mL) under 160 mW/cm² light irradiation with a 300 W Xe lamp and mechanical
37 stirring. Then the reaction was initiated by adding 7.8 mg NH₃BH₃.
38
39
40
41
42
43

44 Catalytic performance evaluation of CuPd@ZIF-8 or CuPd for hydrogenation of
45 phenylacetylene and phenylethylene in the presence of NH₃BH₃: Typically, a mixture of 1 mg
46 CuPd@ZIF-8 (1 mL, 1 mg/mL), 0.1 mmol phenylacetylene, 5 mL methanol was placed in a two-
47 necked round-bottomed flask (25 mL) under 160 mW/cm² light irradiation with a 300 W Xe
48 lamp and mechanical stirring. The reaction was initiated after adding 7.8 mg NH₃BH₃ and
49
50
51
52
53
54
55
56
57
58
59
60

1
2
3 proceeded for 10 min. After the reaction completion, 200 μL of the resultant mixture was taken
4
5 into a mixed solvent with 1 mL H_2O and 1 mL ethyl acetate. Upon the adequate shaking, the
6
7 mixture was allowed to be centrifuged and the product was extracted to the upper layer of ethyl
8
9 acetate. Then, 600 μL of sample in the upper solution was detected by GC. For the catalytic
10
11 recycling experiments, CuPd@ZIF-8 was separated by centrifugation after reaction, being
12
13 thoroughly washed by 5 mL methanol for 3 times. Then, it was dried in vacuum for 6 h for the
14
15 next run. The hydrogenation of phenylethylene was attempted under similar conditions.
16
17
18

19 For the reaction with CuPd NCs, 5 mg of CuPd NCs were measured accurately, then dispersed
20
21 into 5 mL methanol, giving the CuPd solution with the concentration of ~ 1 mg/mL. Then, 16.5
22
23 μL of CuPd catalyst (1 mg/mL) was took out and mixed with the 0.1 mmol phenylacetylene and
24
25 5 mL methanol in a two-necked round-bottomed flask (25 mL) under 160 mW/cm^2 light
26
27 irradiation with a 300 W Xe lamp and mechanical stirring. The reaction was initiated after
28
29 adding 7.8 mg NH_3BH_3 and proceeded for 10 min. After the reaction completion, 200 μL of the
30
31 resultant mixture was taken into a mixed solvent with 1 mL H_2O and 1 mL ethyl acetate. Upon
32
33 the adequate shaking, the mixture was allowed to be centrifuged and the product was extracted to
34
35 the upper layer of ethyl acetate. Then, 600 μL of sample in the upper solution was detected by
36
37 GC.
38
39
40
41

42 **Catalytic performance evaluation of CuPd@ZIF-8 for hydrogenation of phenylacetylene**
43
44 **by H_2 gas:** The hydrogenation of phenylacetylene in H_2 atmosphere was proceeded as follows.
45
46 Typically, a mixture of 1 mg CuPd@ZIF-8 (1 mL, 1 mg/mL), 0.1 mmol phenylacetylene and 5
47
48 mL methanol was placed in a necked round-bottomed flask (25 mL) with a H_2 balloon. The
49
50 reaction was accelerated under 160 mW/cm^2 light irradiation with a 300 W Xe lamp.
51
52
53
54
55
56
57
58
59
60

Catalytic performance evaluation of CuPd@ZIF-8 and CuPd for hydrogenation of phenylpropionaldehyde in the presence of NH_3BH_3 : Typically, a mixture of CuPd@ZIF-8 (1 mL, 1 mg/mL) or equimolar amount of CuPd (18.8 μL , 2 mg/mL), 0.1 mmol phenylpropionaldehyde, 4.5 mL methanol and 1.5 mL H_2O were placed in a two-necked round-bottomed flask (25 mL) under 160 mW/cm^2 light irradiation with a 300 W Xe lamp and mechanical stirring. Then the reaction was initiated by adding 7.8 mg NH_3BH_3 .

Time-dependent conversion of phenylacetylene or phenylethylene hydrogenation: Typically, a mixture of 1 mg CuPd@ZIF-8 (1 mL, 1 mg/mL), 0.1 mmol phenylacetylene or phenylethylene, 5 mL methanol was placed in a two-necked round-bottomed flask (25 mL) under 160 mW/cm^2 light irradiation with a 300 W Xe lamp under mechanical stirring. Then the reaction was initiated by adding 7.8 mg NH_3BH_3 . To obtain the kinetic curve of the catalytic reaction, during the reaction process, 80 μL of the reaction mixture was sampled per 30 seconds.

Dependency of the reaction rate on the amount of NH_3BH_3 : A mixture of 1 mg CuPd@ZIF-8 (1 mL, 1 mg/mL), 0.1 mmol phenylacetylene or phenylethylene, 5 mL methanol was placed in a two-necked round-bottomed flask (25 mL) under 160 mW/cm^2 light irradiation with a 300 W Xe lamp under mechanical stirring. Then, different amount of NH_3BH_3 was added to initiate the reaction and the time-dependent conversion was completed following as the above process, respectively.

Deuterium-labeling experiments: All controlled experiments were completed under the same conditions as the experiment above except for that the substrate or reactant was replaced by the corresponding deuterated reagent.

DFT Calculation Method: The Perdew-Burke-Ernzerhof (PBE) functional and projector augmented wave (PAW) potentials were adopted to complete the DFT calculations by using

1
2
3 Vienna *ab initio* simulation package.^{69, 70} In detail, the spin polarization correction was included
4
5 to consider the magnetism effect. Consistent with previous studies,^{71, 72} a $1\times 1\times 1$ Γ -centered k -
6
7 point and 500 eV cutoff energy were adopted to obtain accurate electronic energy in ground-state.
8
9
10 The convergence standards of energy and force were selected as 10^{-5} eV and 0.02 eV/Å. The
11
12 vibrational frequency with finite displacements of ± 0.02 Å was calculated to obtain the zero
13
14 point energy correction and vibrational entropy correction.
15

16 ASSOCIATED CONTENT

17 18 19 20 **Supporting Information**

21
22 The Supporting Information is available free of charge at

23
24 https://pubs.acs.org/doi/10.1021/*****.

25
26
27 Materials and instrumentation; material characterizations and catalytic results.

28 29 30 AUTHOR INFORMATION

31 32 **Corresponding Author**

33
34
35 *E-mail: jianglab@ustc.edu.cn

36 37 38 **Author Contributions**

39
40 The manuscript was written through contributions of both authors. Both authors have given
41
42 approval to the final version of the manuscript.
43
44

45 46 **Notes**

47
48 The authors declare no competing financial interest.
49
50
51
52
53
54
55
56
57
58
59
60

ACKNOWLEDGMENT

We gratefully thank all reviewers for their insightful comments and valuable suggestions. This work was supported by the National Natural Science Foundation of China (21725101, 21871244, 21673213, 21521001), International Partnership Program of CAS (211134KYSB20190109), Fundamental Research Funds for the Central Universities (WK2060030029), and Fujian Institute of Innovation (CAS).

REFERENCES

- (1) Studt, F.; Abild-Pedersen, F.; Bligaard, T.; Sørensen, R. Z.; Christensen, C. H.; Nørskov, J. K. Identification of Non-Precious Metal Alloy Catalysts for Selective Hydrogenation of Acetylene. *Science* **2008**, *320*, 1320-1322.
- (2) Mitsudome, T.; Takahashi, Y.; Ichikawa, S.; Mizugaki, T.; Jitsukawa, K.; Kaneda, K. Metal-Ligand Core-Shell Nanocomposite Catalysts for the Selective Semihydrogenation of Alkynes. *Angew. Chem. Int. Ed.* **2013**, *52*, 1481-1485.
- (3) Huang, F.; Deng, Y.; Chen, Y.; Cai, X.; Peng, M.; Jia, Z.; Ren, P.; Xiao, D.; Wen, X.; Wang, N.; Liu, H.; Ma, D. Atomically Dispersed Pd on Nanodiamond/Graphene Hybrid for Selective Hydrogenation of Acetylene. *J. Am. Chem. Soc.* **2018**, *140*, 13142-13146.
- (4) Chinchilla, R.; Nájera, C. Chemicals from Alkynes with Palladium Catalysts. *Chem. Rev.* **2014**, *114*, 1783-1826.
- (5) Li, G.; Jin, R. Gold Nanocluster-Catalyzed Semihydrogenation: A Unique Activation Pathway for Terminal Alkynes. *J. Am. Chem. Soc.* **2014**, *136*, 11347-11354.

1
2
3 (6) Albani, D.; Shahrokhi, M.; Chen, Z.; Mitchell, S.; Hauert, R.; Lopez, N.; Pérez-Ramírez, J.
4 Selective Ensembles in Supported Palladium Sulfide Nanoparticles for Alkyne Semi-
5 hydrogenation. *Nat. Commun.* **2018**, *9*, 2634.
6
7

8
9
10
11 (7) Trotus, I.-T.; Zimmermann, T.; Schüth, F. Catalytic Reactions of Acetylene: A Feedstock for
12 the Chemical Industry Revisited. *Chem. Rev.* **2014**, *114*, 1761-1782.
13
14
15

16
17 (8) Yang, L.; Jin, Y.; Fang, X.; Cheng, Z.; Zhou, Z. Magnetically Recyclable Core-Shell
18 Structured Pd-Based Catalysts for Semihydrogenation of Phenylacetylene. *Ind. Eng. Chem. Res.*
19 **2017**, *56*, 14182-14191.
20
21
22

23
24 (9) Ji, S.; Chen, Y.; Zhao, S.; Chen, W.; Shi, L.; Wang, Y.; Dong, J.; Li, Z.; Li, F.; Chen, C.;
25 Peng, Q.; Li, J.; Wang, D.; Li, Y. Atomically Dispersed Ruthenium Species Inside Metal-
26 Organic Frameworks: Combining the High Activity of Atomic Sites and the Molecular Sieving
27 Effect of MOFs. *Angew. Chem. Int. Ed.* **2019**, *58*, 4271-4275.
28
29
30
31
32

33
34 (10) Hoyt, C. B.; Sarazen, M. L.; Jones, C. W. Hydroboration of Substituted Alkynes using a
35 Solid Polymeric Carboxylic Acid Catalyst. *J. Catal.* **2019**, *369*, 493-300.
36
37
38

39
40 (11) Christopher, M. K.; Joel, D. K.; Michael, T. Selective Hydrogenation of Acetylene to
41 Ethylene in the Presence of a Carbonaceous Surface Layer on a Pd/Cu (111) Single-Atom Alloy.
42 *ACS Catal.* **2017**, *7*, 8042-8049.
43
44
45
46

47
48 (12) Cao, X.; Fu, Q.; Luo, Y. Catalytic Activity of Pd-Doped Cu Nanoparticles for
49 Hydrogenation as a Single-Atom-Alloy Catalyst. *Phys. Chem. Chem. Phys.* **2014**, *16*, 8367-8375.
50
51
52
53
54
55
56
57
58

1
2
3 (13) Kyriakou, G.; Boucher, M. B.; Jewell, A. D.; Lewis, E. A.; Lawton, T. J.; Baber, A. E.;
4 Tierney, H. L.; Flytzani-Stephanopoulos, M.; Sykes, E. C. H. Isolated Metal Atom Geometries as
5 a Strategy for Selective Heterogeneous Hydrogenations. *Science* **2012**, *335*, 1209-1212.
6
7

8
9
10
11 (14) Pei, G. X.; Liu, X. Y.; Yang, X.; Zhang, L.; Wang, A.; Li, L.; Wang, H.; Wang, X.; Zhang,
12 T. Performance of Cu-Alloyed Pd Single-Atom Catalyst for Semihydrogenation of Acetylene
13 under Simulated Front-End Conditions. *ACS Catal.* **2017**, *7*, 1491-1500.
14
15

16
17
18
19 (15) Silva, F. P.; Fiorio, J. L.; Goncalves, R. V.; Teixeira-Neto, E.; Rossi, L. M. Synergic Effect
20 of Copper and Palladium for Selective Hydrogenation of Alkynes. *Ind. Eng. Chem. Res.* **2018**,
21 *57*, 16209-16216.
22
23

24
25
26
27 (16) Guo, X.; Hao, C.; Jin, G.; Zhu, H.-Y.; Guo, X.-Y. Copper Nanoparticles on Graphene
28 Support: An Efficient Photocatalyst for Coupling of Nitroaromatics in Visible Light. *Angew.*
29 *Chem. Int. Ed.* **2014**, *53*, 1973-1977.
30
31

32
33
34
35 (17) Wang, F.; Li, C.; Chen, H.; Jiang, R.; Sun, L.-D.; Li, Q.; Wang, J.; Yu, J. C.; Yan, C.-H.
36 Plasmonic Harvesting of Light Energy for Suzuki Coupling Reactions. *J. Am. Chem. Soc.* **2013**,
37 *135*, 5588-5601.
38
39

40
41
42
43 (18) Liz-Marzán, L. M.; Murphy, C. J.; Wang, J. Nanoplasmonics. *Chem. Soc. Rev.* **2014**, *43*,
44 3820-3822.
45
46

47
48
49 (19) Chen, Y.-Z.; Wang, Z. U.; Wang, H.; Lu, J.; Jiang, H.-L. Singlet Oxygen-Engaged Selective
50 Photo-Oxidation over Pt Nanocrystals/Porphyrinic MOF: The Roles of Photothermal Effect and
51 Pt Electronic State. *J. Am. Chem. Soc.* **2017**, *139*, 2035-2044.
52
53
54

1
2
3 (20) Hung, L.-I.; Tsung, C.-K.; Huang, W.; Yang, P. Room-Temperature Formation of Hollow
4 Cu₂O Nanoparticles. *Adv. Mater.* **2010**, *22*, 1910-1914.
5
6

7
8 (21) Sarkar, C.; Pendem, S.; Shrotri, A.; Dao, D. Q.; Mai, P. P. T.; Ngoc, T. N.; Chandaka, D. R.;
9 Rao, T. V.; Trinh, Q. T.; Sherburne, M. P.; Mondal, J. Interface Engineering of Graphene-
10 Supported Cu Nanoparticles Encapsulated by Mesoporous Silica for Size-Dependent Catalytic
11 Oxidative Coupling of Aromatic Amines. *ACS Appl. Mater. Interfaces* **2019**, *11*, 11722-11735.
12
13
14
15

16 (22) Furukawa, H.; Cordova, K. E.; O'Keeffe, M.; Yaghi, O. M. The Chemistry and
17 Applications of Metal-Organic Frameworks. *Science* **2013**, *341*, 1230444.
18
19
20
21

22 (23) Zhou, H.-C.; Kitagawa, S. Metal-Organic Frameworks (MOFs). *Chem. Soc. Rev.* **2014**, *43*,
23 5415-5418.
24
25
26
27

28 (24) Islamoglu, T.; Goswami, S.; Li, Z.; Howarth, A. J.; Farha, O. K.; Hupp, J. T. Postsynthetic
29 Tuning of Metal-Organic Frameworks for Targeted Applications. *Acc. Chem. Res.* **2017**, *50*,
30 805-813.
31
32
33
34
35

36 (25) Li, B.; Wen, H.-M.; Cui, Y.; Zhou, W.; Qian, G.; Chen, B. Emerging Multifunctional Metal-
37 Organic Framework Materials. *Adv. Mater.* **2016**, *28*, 8819-8860.
38
39
40
41

42 (26) Zhao, X.; Wang, Y.; Li, D.; Bu, X.; Feng, P. Metal-Organic Frameworks for Separation.
43 *Adv. Mater.* **2018**, *30*, 1705189.
44
45
46
47

48 (27) Li, G.; Zhao, S.; Zhang, Y.; Tang, Z. Metal-Organic Frameworks Encapsulating Active
49 Nanoparticles as Emerging Composites for Catalysis: Recent Progress and Perspectives. *Adv.*
50 *Mater.* **2018**, *30*, 1800702.
51
52
53
54
55

1
2
3 (28) Kirchon, A.; Feng, L.; Drake, H. F.; Joseph, E. A.; Zhou, H.-C. From Fundamentals to
4 Applications: a Toolbox for Robust and Multifunctional MOF Materials. *Chem. Soc. Rev.* **2018**,
5
6 47, 8611-8638.
7

8
9
10
11 (29) Zhang, D.; Zhu, Y.; Liu, L.; Ying, X.; Hsiung, C.-E.; Sougrat, R.; Li, K.; Han, Y. Atomic-
12 Resolution Transmission Electron Microscopy of Electron Beam-Sensitive Crystalline Materials.
13
14 *Science* **2018**, 359, 675-679.
15

16
17
18 (30) Luo, Y.-H.; Dong, L.-Z.; Liu, J.; Li, S.-L.; Lan, Y.-Q. From Molecular Metal Complex to
19 Metal-Organic Framework: The CO₂ Reduction Photocatalysts with Clear and Tunable
20 Structure. *Coord. Chem. Rev.* **2019**, 390, 86-126.
21
22

23
24
25 (31) Rungtaweeworanit, B.; Baek, J.; Araujo, J. R.; Archanjo, B. S.; Choi, K. M.; Yaghi, O. M.;
26 Somorjai, G. A. Copper Nanocrystals Encapsulated in Zr-based Metal-Organic Frameworks for
27 Highly Selective CO₂ Hydrogenation to Methanol. *Nano Lett.* **2016**, 16, 7645-7649.
28
29

30
31
32 (32) Yang, Q.; Xu, Q.; Yu, S.-H.; Jiang, H.-L. Pd Nanocubes@ZIF-8: Integration of
33 Plasmon-Driven Photothermal Conversion with a Metal-Organic Framework for Efficient and
34 Selective Catalysis. *Angew. Chem. Int. Ed.* **2016**, 55, 3685-3689.
35
36

37
38 (33) Zhang, W.; Zheng, B.; Shi, W.; Chen, X.; Xu, Z.; Li, S.; Chi, Y. R.; Yang, Y.; Lu, J.;
39 Huang, W.; Huo, F. Site-Selective Catalysis of a Multifunctional Linear Molecule: The Steric
40 Hindrance of Metal-Organic Framework Channels. *Adv. Mater.* **2018**, 30, 1800643.
41
42

43
44 (34) Li, X.; Zhang, B.; Tang, L.; Goh, T. W.; Qi, S.; Volkov, A.; Pei, Y.; Qi, Z.; Tsung, C.-K.;
45 Stanley, L.; Huang, W. Cooperative Multifunctional Catalysts for Nitrene Synthesis: Platinum
46
47
48
49

1
2
3 Nanoclusters in Amine-Functionalized Metal-Organic Frameworks. *Angew. Chem. Int. Ed.* **2017**,
4
5 *56*, 16371-16375.

6
7
8
9 (35) Yang, Q.; Xu, Q.; Jiang, H.-L. Metal-Organic Frameworks Meet Metal Nanoparticles:
10
11 Synergistic Effect for Enhanced Catalysis. *Chem. Soc. Rev.* **2017**, *46*, 4774-4808.

12
13
14 (36) Huang, Y.-B.; Liang, J.; Wang, X.-S.; Cao, R. Multifunctional Metal-Organic Framework
15
16 Catalysts: Synergistic Catalysis and Tandem Reactions. *Chem. Soc. Rev.* **2017**, *46*, 126-157.

17
18
19 (37) Hu, P.; Morabito, J. V.; Tsung, C.-K. Core-Shell Catalysts of Metal Nanoparticle Core and
20
21 Metal-Organic Framework Shell. *ACS Catal.* **2014**, *4*, 4409-4419.

22
23
24
25 (38) Rogge, S. M. J.; Bavykina, A.; Hajek, J.; Garcia, H.; Olivos-Suarez, A. I.; Sepulveda-
26
27 Escribano, A.; Vimont, A.; Clet, G.; Bazin, P.; Kapteijn, F.; Daturi, M.; Ramos-Fernandez, E. V.;
28
29 Llabres, I. X. F. X.; Van Speybroeck, V.; Gascon, J. Metal-Organic and Covalent Organic
30
31 Frameworks as Single-Site Catalysts. *Chem. Soc. Rev.* **2017**, *46*, 3134-3184.

32
33
34
35 (39) Zhao, M.; Ou, S.; Wu, C.-D. Porous Metal-Organic Frameworks for Heterogeneous
36
37 Biomimetic Catalysis. *Acc. Chem. Res.* **2014**, *47*, 1199-1207.

38
39
40
41 (40) Lee, K. J.; Lee, J. H.; Jeoung, S.; Moon, H. R. Transformation of Metal-Organic
42
43 Frameworks/Coordination Polymers into Functional Nanostructured Materials: Experimental
44
45 Approaches Based on Mechanistic Insights. *Acc. Chem. Res.* **2017**, *50*, 2684-2692.

46
47
48
49 (41) Khaletskaya, K.; Reboul, J.; Meilikhov, M.; Nakahama, M.; Diring, S.; Tsujimoto, M.;
50
51 Isoda, S.; Kim, F.; Kamei, K. I.; Fischer, R. A.; Kitagawa, S.; Furukawa, S. Integration of Porous
52
53

1
2
3 Coordination Polymers and Gold Nanorods into Core-Shell Mesoscopic Composites toward
4 Light-Induced Molecular Release. *J. Am. Chem. Soc.* **2013**, *135*, 10998-11005.
5
6

7
8
9 (42) Wang, C.; An, B.; Lin, W. Metal-Organic Frameworks in Solid-Gas Phase Catalysis. *ACS*
10 *Catal.* **2019**, *9*, 130-146.
11

12
13
14 (43) Zhai, Q.; Bu, X.; Zhao, X.; Li, D.; Feng, P. Pore Space Partition in Metal-Organic
15 Frameworks. *Acc. Chem. Res.* **2017**, *50*, 407-417.
16
17

18
19
20 (44) Hermes, S.; Schröter, M.-K.; Schmid, R.; Khodeir, L.; Muhler, M.; Tissler, A.; Fischer, R.
21 W.; Fischer, R. A. Metal@ MOF: Loading of Highly Porous Coordination Polymers Host
22 Lattices by Metal Organic Chemical Vapor Deposition. *Angew. Chem. Int. Ed.* **2005**, *44*, 6237-
23 6241.
24
25
26
27

28
29
30 (45) Liu, H.; Chang, L.; Bai, C.; Chen, L.; Luque, R.; Li, Y. Controllable Encapsulation of
31 “Clean” Metal Clusters within Mofs Through Kinetic Modulation: towards Advanced
32 Heterogeneous Nanocatalysts. *Angew. Chem. Int. Ed.* **2016**, *55*, 5019-5023.
33
34
35

36
37
38 (46) Dhakshinamoorthy, A.; Garcia, H. Catalysis by Metal Nanoparticles Embedded on Metal-
39 Organic Frameworks. *Chem. Soc. Rev.* **2012**, *41*, 5262-5284.
40
41

42
43
44 (47) Zhao, M.; Yang, K.; Wang, Y.; Li, G.; Guo, J.; Gu, L.; Hu, W.; Zhao, H.; Tang, Z. Metal-
45 Organic Frameworks as Selectivity Regulators for Hydrogenation Reactions. *Nature* **2016**, *539*,
46 76-80.
47
48
49

50
51 (48) Choe, K.; Zheng, F.; Wang, H.; Yuan, Y.; Zhao, W.; Xue, G.; Qiu, X.; Ri, M.; Shi, X.;
52 Wang, Y.; Li, G.; Tang, Z. Fast and Selective Semihydrogenation of Alkynes by Palladium
53
54
55
56
57

1
2
3 Nanoparticles Sandwiched in Metal-Organic Frameworks. *Angew. Chem. Int. Ed.* **2020**, *59*,
4 3650-3657.
5
6

7
8
9 (49) Park, K. S.; Ni, Z.; Côté, A. P.; Choi, J. Y.; Huang, R.; Uribe-Romo, F. J.; Chae, H. K.;
10 O’Keeffe, M.; Yaghi, O. M. Exceptional Chemical and Thermal Stability of Zeolitic Imidazolate
11 Frameworks. *Proc. Natl. Acad. Sci. U.S.A.* **2006**, *103*, 10186-10191.
12
13

14
15
16 (50) Huang, X.-C.; Lin, Y.-Y.; Zhang, J.-P.; Chen, X.-M. Ligand-Directed Strategy for Zeolite-
17 Type Metal-Organic Frameworks: Zinc (II) Imidazolates with Unusual Zeolitic Topologies.
18
19 *Angew. Chem. Int. Ed.* **2006**, *45*, 1557-1559.
20
21

22
23
24 (51) Jin, M.; He, G.; Zhang, H.; Zeng, J.; Xie, Z.; Xia, Y. Shape-Controlled Synthesis of Copper
25 Nanocrystals in an Aqueous Solution with Glucose as a Reducing Agent and Hexadecylamine as
26 a Capping Agent. *Angew. Chem. Int. Ed.* **2011**, *50*, 10560-10564.
27
28

29
30
31 (52) McCue, A. J.; McRitchie, C. J.; Shepherd, A. M.; Anderson, J. A. Cu/Al₂O₃ Catalysts
32 Modified with Pd for Selective Acetylene Hydrogenation. *J. Catal.* **2014**, *319*, 127-135.
33
34

35
36
37 (53) Rodríguez-Kessler, P. L.; Alonso-Dávila, P.; Navarro-Santos, P.; Morato-Márquez, J. A.;
38 Ortíz-Chi, F.; Rodríguez-Domínguez, A. R. Hydrogen Chemisorption on Pd-Doped Copper
39 Clusters. *J. Phys. Chem. C* **2019**, *123*, 15834-15840.
40
41

42
43
44 (54) Zhan, W.-W.; Zhu, Q.-L.; Xu, Q. Dehydrogenation of Ammonia Borane by Metal
45 Nanoparticle Catalysts. *ACS Catal.* **2016**, *6*, 6892-6905.
46
47

48
49
50 (55) Demirci, U. B.; Miele, P. Sodium Borohydride versus Ammonia Borane, in Hydrogen
51 Storage and Direct Fuel Cell Applications. *Energy Environ. Sci.* **2009**, *2*, 627-637.
52
53

1
2
3 (56) He, T.; Pachfule, P.; Wu, H.; Xu, Q.; Chen, P. Hydrogen Carrier. *Nat. Rev. Mater.* **2016**, *1*,
4
5 16059.

6
7
8 (57) Yang, Q.; Chen, Y.-Z.; Wang, Z. U.; Xu, Q.; Jiang, H.-L. One-Pot Tandem Catalysis over
9
10 Pd@MIL-101: Boosting the Efficiency of Nitro Compound Hydrogenation by Coupling with
11
12 Ammonia Borane Dehydrogenation. *Chem. Commun.* **2015**, *51*, 10419-10422.

13
14
15 (58) Shen, M.; Liu, H.; Yu, C.; Yin, Z.; Muzzio, M.; Li, J.; Xi, Z.; Yu, Y.; Sun, S. Room-
16
17 Temperature Chemoselective Reduction of 3-Nitrostyrene to 3-Vinylniline by Ammonia
18
19 Borane over Cu Nanoparticles. *J. Am. Chem. Soc.* **2018**, *140*, 16460-16463.

20
21
22 (59) Han, C.; Meng, P.; Waclawik, E. R.; Zhang, C.; Li, X.-H.; Yang, H.; Antonietti, M.; Xu, J.
23
24 Palladium/Graphitic Carbon Nitride (g-C₃N₄) Stabilized Emulsion Microreactor as a Store for
25
26 Hydrogen from Ammonia Borane for Use in Alkene Hydrogenation. *Angew. Chem. Int. Ed.*
27
28 **2018**, *57*, 14857-14861.

29
30
31 (60) Fu, S.; Chen, N.-Y.; Liu, X.; Shao, Z.; Luo, S.-P.; Liu, Q. Ligand-Controlled Cobalt-
32
33 Catalyzed Transfer Hydrogenation of Alkynes: Stereodivergent Synthesis of Z- and E-Alkenes.
34
35 *J. Am. Chem. Soc.* **2016**, *138*, 8588-8594.

36
37
38 (61) Rej, S.; Madasu, M.; Tan, C.-S.; Hsia, C.-F.; Huang, M. H. Polyhedral Cu₂O to Cu
39
40 Pseudomorphic Conversion for Stereoselective Alkyne Semihydrogenation. *Chem. Sci.* **2018**, *9*,
41
42 2517-2524.

43
44
45 (62) Mitsudome, T.; Yamamoto, M.; Maeno, Z.; Mizugaki, T.; Jitsukawa, K.; Kaneda, K. One-
46
47 Step Synthesis of Core-Gold/Shell-Ceria Nanomaterial and Its Catalysis for Highly Selective
48
49 Semihydrogenation of Alkynes. *J. Am. Chem. Soc.* **2015**, *137*, 13452-13455.

1
2
3 (63) Li, Z.; He, T.; Liu, L.; Chen, W.; Zhang, M.; Wu, G.; Chen, P. Covalent Triazine
4 Framework Supported Non-Noble Metal Nanoparticles with Superior Activity for Catalytic
5 Hydrolysis of Ammonia Borane: from Mechanistic Study to Catalyst Design. *Chem. Sci.* **2017**, *8*,
6 781-788.
7
8
9

10
11
12
13 (64) Vasilikogiannaki, E.; Titilas, I.; Vassilikogiannakis, G.; Stratakis, M. *cis*-
14 Semihydrogenation of Alkynes with Amine Borane Complexes Catalyzed by Gold Nanoparticles
15 under Mild Conditions. *Chem. Commun.* **2015**, *51*, 2384-2387.
16
17
18
19

20
21 (65) Finšgar, M.; Jackson, J. Application of Corrosion Inhibitors for Steels in Acidic Media for
22 the Oil and Gas Industry: A Review. *Corros. Sci.* **2014**, *86*, 17-41.
23
24
25

26
27 (66) Chen, L.; Peng, Y.; Wang, H.; Gu, Z.; Duan, C. Synthesis of Au@ ZIF-8 Single- or Multi-
28 Core-Shell Structures for Photocatalysis. *Chem. Commun.* **2014**, *50*, 8651-8654.
29
30
31

32 (67) Jin, M.; Liu, H.; Zhang, H.; Xie, Z.; Liu, J.; Xia, Y. Synthesis of Pd Nanocrystals Enclosed
33 by {100} Facets and with Sizes <10 nm for Application in CO Oxidation. *Nano Res.* **2011**, *4*, 83-
34 91.
35
36
37
38

39
40 (68) Ramachandran, P. V.; Gagare, P. D. Preparation of Ammonia Borane in High Yield and
41 Purity, Methanolysis, and Regeneration. *Inorg. Chem.* **2007**, *46*, 7810-7817.
42
43
44

45
46 (69) Perdew, J. P.; Burke, K.; Ernzerhof, M. Generalized Gradient Approximation Made Simple.
47 *Phys. Rev. Lett.* **1996**, *77*, 3865-3868.
48
49
50

51 (70) Kresse, G.; Furthmüller, J. Efficiency of Ab-Initio Total Energy Calculations for Metals and
52 Semiconductors Using A Plane-Wave Basis Set. *Comput. Mater. Sci.* **1996**, *6*, 15-50.
53
54
55

1
2
3 (71) Gao, Z. Y.; Yang, W. J.; Ding, X. L.; Lv, G.; Yan, W. P. Support Effects on Adsorption and
4 Catalytic Activation of O₂ in Single Atom Iron Catalysts with Graphene-Based Substrates. *Phys.*
5
6 *Chem. Chem. Phys.* **2018**, *20*, 7333-7341.
7
8
9

10
11 (72) Yang, W.; Gao, Z.; Liu, X.; Li, X.; Ding, X.; Yan, W. Single-Atom Iron Catalyst with
12
13 Single-Vacancy Graphene-Based Substrate as A Novel Catalyst for NO Oxidation: A Theoretical
14
15
16 Study. *Catal. Sci. Technol.* **2018**, *8*, 4159-4168.
17
18
19
20
21
22
23
24
25
26
27
28
29
30
31
32
33
34
35
36
37
38
39
40
41
42
43
44
45
46
47
48
49
50
51
52
53
54
55
56
57
58
59
60

Table of Contents

A core-shell MOF composite, CuPd@ZIF-8 featuring cubic Cu supported Pd nanoparticles together as a core, is rationally fabricated. The CuPd@ZIF-8 exhibits high activity and selectivity for alkyne hydrogenation, where Cu regulates chemoselectivity of Pd sites and generates photothermal effect to boost the reaction, ZIF-8 provides regioselectivity and stabilizes CuPd and NH_3BH_3 generating *in-situ* H species contributes to the high chemoselectivity.

